

Stratification-induced scale splitting in convection

O. V. Shcheritsa^{a,*}, A. V. Getling^b, O. S. Mazhorova^a

^a*Keldysh Institute of Applied Mathematics, Moscow, 125047 Russia*

^b*Skobeltsyn Institute of Nuclear Physics, Lomonosov Moscow State University,
Moscow, 119991 Russia*

Abstract

The coexistence of motions on various scales is a remarkable feature of solar convection, which should be taken into account in analyses of the dynamics of magnetic fields. Therefore, it is important to investigate the factors responsible for the observed multiscale structure of solar convection. In this study, an attempt is made to understand how the scales of convective motions are affected by the particularities of the static temperature stratification of a fluid layer. To this end, simple models are considered. The equations of two-dimensional thermal convection are solved numerically for a plane horizontal fluid layer heated from below, in an extended Boussinesq approximation that admits thermal-diffusivity variations. These variations specify the stratification of the layer. The static temperature gradient in a thin sublayer near the upper surface of the layer is assumed to be many times larger than in the remainder of the layer. In some cases, distributed heat sinks are assumed to produce a stably stratified region overlying the convective layer. Manifestations of the scale-splitting effect are noted, which depend on the boundary conditions and stratification. Small-scale convection cells are carried by larger-scale flows. In particular, the phase trajectories of fluid particles indicate the presence of complex attractors, which reflect the multiscale structure of the flow. The effect of the stably stratified upper sublayer on the flow scales is also considered.

Keywords:

multiscale convection; temperature stratification

1. Introduction

The dynamics of solar magnetic fields depends crucially on the structure of the velocity field in the convection zone. In particular, the coexistence of convective motions on various scales is clearly reflected by the magnetic-field structure on the photospheric levels.

At least four types of cellular structures, strongly differing in their scale, can be identified with certainty on the solar surface and attributed to the phenomenon of thermal convection, i.e., granules, mesogranules, supergranules, and giant cells. This multiscale structure is an important feature of solar convection, which should be taken into account in studying the dynamics of

*Corresponding author

Email addresses: shchery@mail.ru (O. V. Shcheritsa), A.Getling@mail.ru (A. V. Getling), olgamazhor@mail.ru (O. S. Mazhorova)

magnetic fields. It has not yet received a convincing explanation, and an adequate hydrodynamic description must be given to both the spatial structure of the flows and the factors responsible for its development.

It can naturally be expected that, if convection cells are not large in their plan size compared to the full thickness of the convecting fluid layer, they should also be vertically localised in a relatively thin portion of this layer. This is obviously possible if a certain sublayer (height interval) where convection can develop due to an unstable temperature stratification is contiguous with another sublayer where the stratification is stable and exerts a braking action on the convective motion (in this case, the flow nevertheless penetrates into the stable region; i.e., penetrative convection occurs). If, however, the entire layer (from top to bottom) is convectively unstable, the localisation of motion in a relatively thin sublayer is not such a trivial effect. The possibility of the coexistence of small cells with larger ones, filling the entire layer thickness, is even less obvious.

Quite likely, scale splitting could result from sharp changes in the static vertical entropy gradient (or the static temperature gradient in the case of an incompressible fluid) at some heights. Under the conditions of the solar convection zone, there are some prerequisites for manifestations of such an effect, related to the enhanced instability of the sublayers of partial ionization of hydrogen and helium. Indirect indications for scale splitting in layers with a sharp kink in the static temperature profile were found previously in linear problems (Getling, 1976, 1980), and these expectations were substantiated in part by nonlinear numerical computations (Getling & Tikhomolov, 2007). We investigate here possibilities of scale splitting in the framework of such simple models by means of numerically simulating two-dimensional convection flows.

2. Formulation of the problem and numerical technique

Assume that a plane horizontal layer $0 < z < h$ of a viscous, incompressible fluid is heated from below and consider its finite segment $0 < x < L$ in which we shall simulate two-dimensional ($\partial/\partial y = 0$) convection flows. Let the bottom and top boundaries be perfect thermal conductors and let their temperatures be constant and equal to $T_{\text{bot}} = \Delta T > 0$ and $T_{\text{top}} = 0$, respectively. We also assume that the side walls of the region are thermally insulated. The no-slip impermeability conditions are specified at the bottom and side boundaries of the domain. The top boundary may be either rigid (no-slip) or stress-free.

We are interested in situations where the static temperature varies little (by $\delta T \ll \Delta T$) across the main portion of the layer, of thickness $h - \Delta h$, $\Delta h \ll h$ (Sublayer 1), while the most part of the temperature difference, $\Delta T - \delta T$, corresponds to Sublayer 2 with a small thickness Δh , near the upper surface (Fig. 1). To obtain such profiles, we assume the thermal diffusivity to be temperature-dependent:

$$\chi(T) = 1 + aT + bT^n. \quad (1)$$

In some cases, we introduce heat sinks uniformly distributed over the region overlying a certain level $z = z_0$ located in Sublayer 2 to obtain temperature profiles with a minimum at a certain height, so that a stable Sublayer 3 be located above Sublayer 2 (see below). This sublayer is considered to play the role of a “soft boundary,” as do the stable layers located immediately above the temperature minimum in the solar atmosphere. We shall give no attention to the flow structure within this sublayer.

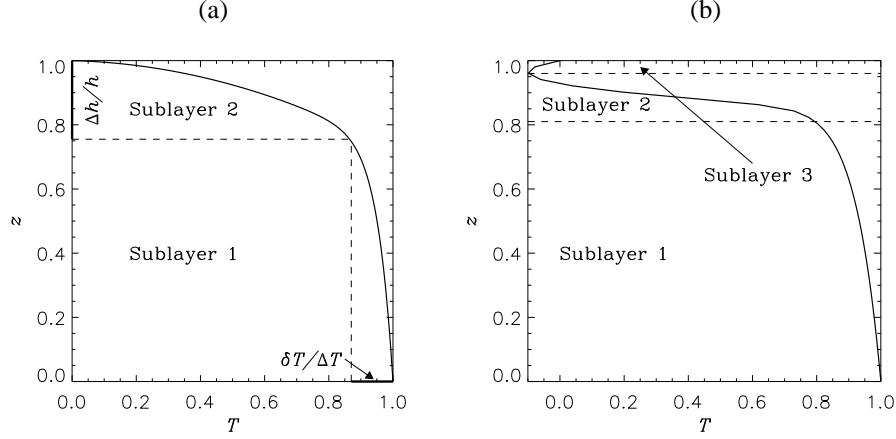


Figure 1: Static temperature profiles (in dimensionless variables): (a) monotonic profile for $a = 20$, $b = 600$, $n = 20$; (b) nonmonotonic profile for $a = 0.01$, $b = 600$, $n = 10$, $q_0 = -2$, $z_0 = 0.8$

To describe the dynamics of convection, we use an extended Boussinesq approximation, which admits thermal-diffusivity variations (for a discussion of different versions of the Boussinesq approximation, see Getling, 1998). If the layer thickness h is chosen as the unit length, ΔT as the unit temperature and the characteristic time of viscous momentum transport, $\tau_v = h^2/\nu$, as the unit time (ν being the kinematic viscosity), the governing equations assume the following dimensionless form:

$$\frac{\partial \mathbf{v}}{\partial t} + (\mathbf{v} \cdot \nabla) \mathbf{v} = -\nabla \varpi + \hat{\mathbf{z}} \frac{R}{P} (T - T_s) + \Delta \mathbf{v}, \quad (2)$$

$$\frac{\partial T}{\partial t} + \mathbf{v} \cdot \nabla T = \frac{1}{P} \nabla \cdot \frac{\chi(T)}{\chi(T_{\text{top}})} \nabla T, \quad (3)$$

$$\nabla \cdot \mathbf{v} = 0; \quad (4)$$

here, $\hat{\mathbf{z}}$ is the z -directed unit vector, $T_s(z)$ is the static temperature distribution, $\chi(T)$ is the thermal diffusivity, ϖ is the nondimensionalised pressure and

$$R = \frac{\alpha g \Delta T h^3}{\nu \chi(T_{\text{top}})} \quad \text{and} \quad P = \frac{\nu}{\chi(T_{\text{top}})}$$

are the Rayleigh and Prandtl numbers, α being the volumetric coefficient of thermal expansion of the fluid and g the gravitational acceleration.

For two-dimensional incompressible flows, the stream function ψ and vorticity ω specified by the equations

$$v_x = \frac{\partial \psi}{\partial z}, \quad v_z = -\frac{\partial \psi}{\partial x}, \quad \omega = -\left(\frac{\partial^2 \psi}{\partial x^2} + \frac{\partial^2 \psi}{\partial z^2} \right)$$

are variables convenient for constructing a computational algorithm. We solve equations (2)–(4) with the chosen boundary conditions using the standard procedure of splitting physical processes (Kovenya & Yanenko, 1981). Specifically, we first employ a matrix algorithm (Mazhorova & Popov,

1980, 1981) to determine the velocity field from (2) written in terms of ψ and ω ; next, we find the temperature distribution in the layer from (3). We use a conservative scheme of the second-order accuracy in the spatial coordinates and of the first-order accuracy in time (Arakawa, 1966). Calculations are carried out on a nonuniform grid, which is finer near the top and bottom layer boundaries. The horizontal size of our computational domain is $L = 5\pi h = 15.7h$, and the total number of nodes is 1024×51 .

Most calculations were done for static temperature profiles specified by dependences (1) with $b = 600$, $a = 10 - 20$, $n = 10 - 80$, the temperature varying monotonically in these cases (Fig. 1a). Alternatively, nonmonotonic profiles (Fig. 1b) were obtained by specifying heat sinks uniformly distributed with a density $-q$ (i.e., negative heat sources with a density q) above the height z_0 , as the solution of the problem

$$\frac{\partial}{\partial z} \left(\chi(T) \frac{\partial T}{\partial z} \right) - q = 0, \quad q = \begin{cases} q_0 < 0, & z > z_0 \\ 0, & z < z_0 \end{cases}.$$

In our simulations, the flow is initiated by introducing random thermal perturbations at a certain height within the upper sublayer.

3. Simulation results

3.1. Monotonic static temperature profiles

For both the no-slip and stress-free boundary conditions on the upper surface of the layer, the critical Rayleigh number R_c was determined in the process of simulation. In the regimes studied, it amounts to $R_c \approx 3.8 \times 10^6$ for a rigid upper boundary and lies in the range $R_c = (4-6) \times 10^5$ for a free upper boundary; the Prandtl number in our calculations is $P = 1$. The qualitative features of the results turn out to be little sensitive to the choice of parameters a and n in the above-mentioned ranges.

If the upper horizontal boundary is rigid, motion starts developing as small-scale convection in Sublayer 2. Later, the disturbances penetrate deeper and gradually involve the entire layer depth. As a result, large-scale convection rolls emerge with a width of about the layer thickness. As this takes place, the small-scale flow in the upper sublayer does not disappear and assumes the form of smaller rolls with a size of about the sublayer thickness. A flow of a similar small scale also develops near the bottom layer boundary. The small rolls are especially pronounced above and below the contact sections of large rolls. Thus, in the fluid layer stratified on the whole unstably, large convection cells¹ filling the entire layer depth coexist with smaller ones localised in relatively thin sublayers (Fig. 2).

To analyse the flow structure, we employ the discrete Fourier transform of the stream function with respect to the horizontal coordinate x at given heights z . High-frequency harmonics are present in the spectrum, whose amplitudes amount to 10–16% of the amplitude of the fundamental mode. To separate the small-scale component of the velocity field and visualise the fine cellular structures present in the flow, we use an ideal low-pass filter (Blahut, 1985) and subtract the obtained large-scale component from the original field (see Fig. 2).

In the case of a free upper boundary, the flow also originates in the upper sublayer, after which the emerged small-scale structures penetrate deeper into the layer, stimulating the formation of a

¹ By a convection cell in a two-dimensional flow, a pair of neighbouring rolls is meant.

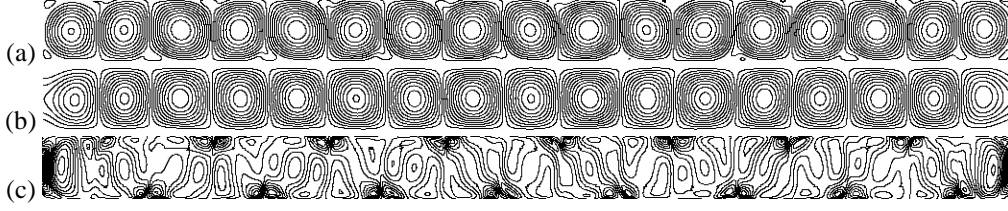


Figure 2: A convective flow computed for a rigid upper boundary and $R = 10R_c$, with large cells and a smaller-scale flow coexisting: (a) stream lines (contours of the stream function); (b) large-scale structures separated from the flow using an ideal low-pass filter; (c) small-scale structures obtained by subtracting the large-scale component from the full stream-function field.

flow throughout the layer. The cells in Sublayer 1 tend to grow in size; however, the small-scale structures present in Sublayer 2 control this process: as the horizontal size of a large structure becomes considerably larger than the layer thickness, the cells moving down from the upper sublayer break this structure into two portions (Fig. 3). In contrast to the case of a rigid upper boundary, where the number of large rolls is constant, the number of large-scale structures in the layer with the free boundary varies between 8 and 16.

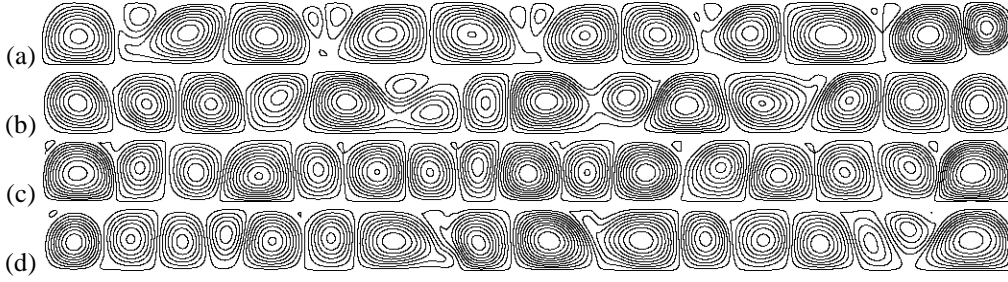


Figure 3: Flow evolution in the case of a free upper boundary, at $R = 1.5R_c$, $P = 1$. Streamlines (contours of the stream function) are shown for different times (measured in the units of the time of viscous momentum transport, τ_v): (a) $t = 0.07$, small-scale cells originating near the upper surface of the layer; (b) $t = 0.09$, a “breaking” effect of the small cells penetrating into the layer depth on those large rolls whose horizontal size considerably exceeds the scale optimum; (c) $t = 0.14$, the flow structure formed in the process of penetration of small cells deeper into the layer; (d) $t = 0.17$, a tendency toward the expansion of large-scale cells. The emergence and development of small-scale structures in the upper sublayer.

The spectrum of the flow is now more complex than in the case of a rigid upper boundary. Since the number of large structures is variable, the fundamental mode is also time dependent. Harmonics with different wavenumbers dominate in the bulk of the layer and in the upper sublayer. The enhancement of the small-scale component frequently parallels with the weakening of the large-scale component, and vice versa — a sort of intermittency is observed. As this takes place, the sublayers in which the cells are localised vary in their thickness and do not coincide with the sublayers specified by the static vertical temperature profile. In contrast to the case of a rigid upper boundary, the small-scale structures are localised only in the upper part of the layer.

3.2. Nonmonotonic static temperature profile

The nonmonotonic static temperature profile shown in Fig. 1b was created by specifying distributed heat sinks in addition to a temperature-dependent thermal diffusivity. The needed

profiles were obtained at the following parameters: $a = 0,01-0,1$, $b = 600$, $n = 10-20$, $q_0 = -2$, $z_0 = 0.8$. In the regimes studied, the Rayleigh number varied in the range $R = 10\,000-200\,000$ and the Prandtl number was $P = 1$. According to very crude estimates based on the computed flow regimes, the critical Rayleigh number is $R_c \sim 13\,000$.

Convection was initiated by introducing a random perturbation of the static temperature profile at a certain height. Motion started developing at the boundary between Sublayers 2 and 3, after which small-scale structures penetrated to deeper levels and stimulated the development of the flow in the bulk of the layer (Fig. 4). Large-scale structures formed, with a vertical size comparable with the layer thickness and horizontal sizes exceeding it. The evolving flow pattern is far from stationary, and the number of large structures varies. Fresh small-scale structures permanently originate at the interface between the sublayers and either glide deeper between two large structures or break a large structure into two parts, preventing it from increasing its horizontal size (Fig. 4b). In the bulk of the layer, local overhear or underheat zones emerge (Figs 4c, 4e), which move relative to one another in a complex way (Fig. 4d).

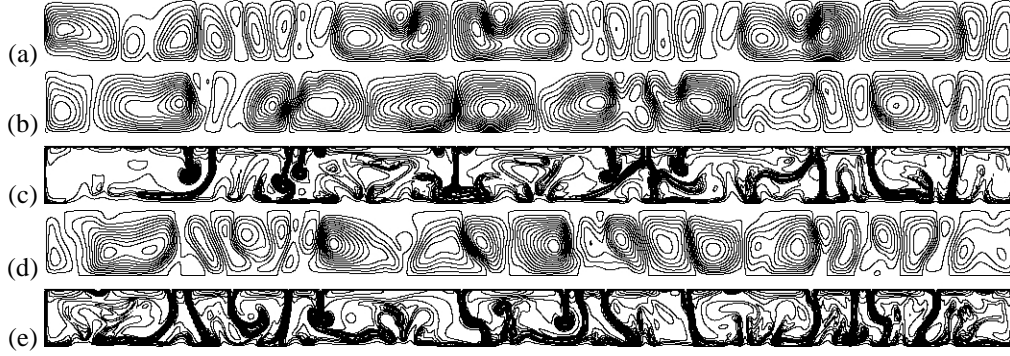


Figure 4: Flow structure in the case of the nonmonotonic static temperature profile, for $R = 20\,000$ and different times (measured in the units of the time of viscous momentum transport, τ_v): (a) stream function at $t = 0.21$, small-scale structures penetrate deep into the layer; (b) stream function at $t = 0.42$, developing small-scale structures either glide deep into the layer or break a large structure into two parts; (c) temperature distribution at $t = 0.42$ with local overhear and underheat zones present in the bulk of the layer; (d) stream function at $t = 0.7$, small-scale structures are transferred by the large ones; (e) temperature distribution at $t = 0.7$ with local overhear and underheat zones present in the bulk of the layer.

It can be seen from the Fourier transform of the stream function that three or four modes (harmonics) with incommensurate wavenumbers dominate in the spectrum of a well-developed flow. The flow is substantially time-dependent, and different modes dominate at different times, so that determining the number of spatial scales present is not a simple task. Applying numerical-homology techniques to the velocity field (Krishan et al., 2007) confirms the coexistence of several spatial scales but does not enable us to determine the size and localisation of the structures.

3.3. Phase space and attractors

The complex structures developing in various flows cannot always be classified and analysed using Fourier-transform-based methods. To make the presence of various flow scales more apparent, we constructed the trajectories of fluid particles in an appropriately defined phase space, (z, v_z) . Several hundred particles differing in their initial position were used. In their motion, all these particles repeatedly passed from one structure to another, and transitions between large

structures and between a large and a small structure — possibly with a subsequent return to the large structure — could take place.

If the static temperature profile is monotonic, an attractor can be detected whose structure clearly demonstrates the presence of different flow scales. In Fig. 5a, which refers to the case of a rigid upper boundary, the trajectory of only one particle is shown, others being quite similar. The velocity vanishes near the upper and lower boundaries ($z = 0$ and $z = 1$) according to the no-slip condition, and a passage of the trajectory from the positive to negative half-plane reflects a transition from ascending to descending motion. Therefore, the large ellipses correspond to a large structure and the small ellipses near $z = 0$ and $z = 1$ represent the small-scale flows near the upper and lower boundaries. If the upper boundary is free, it is near this boundary that small-scale motions are localised (Fig. 5b).

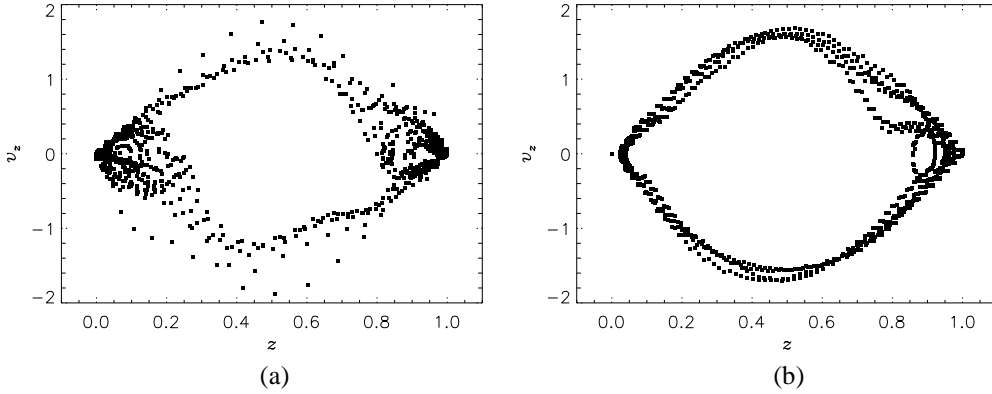


Figure 5: Phase trajectories of a particle in space (z, v_z) : (a) rigid upper boundary; (b) free upper boundary.

It can be found from Fig. 5a that the vertical size of the large structures is equal to the layer thickness h , while the size of the small structure is $0.25h$ near the lower boundary and $0.2h$ near the upper boundary. Different scales of the small structures can be due to different thermal diffusivities near $z = 0$ and $z = 1$: $\chi(T_{\text{bot}}) = 620$, while $\chi(T_{\text{top}}) = 1$. If the upper boundary is free, the vertical size of the small structures is $0.2h$ (Fig. 5b).

Similar analyses were done for the case of a nonmonotonic static temperature profile. The trajectories obtained can be divided into three types (see Fig. 6). The closed loops of the trajectories near $z = 0$ and $z = 1$ evidence the presence of small-scale structures near the upper and lower layer boundaries (Figs 6a, 6b). The trajectory exemplified in Fig. 6c indicates the presence of small-scale structures in the bulk of the layer. Thus, the coexistence of large-scale and small-scale cells can be revealed in the problem with a nonmonotonic static temperature profile, and the small-scale structures are distributed over the whole layer thickness rather than localised in thin sublayers. They move through the layer, being likely carried by the large-scale flow. It should be noted that the spatial trajectories of the particles have numerous nearly horizontal segments, which is reflected by the discontinuities of the phase trajectories seen in Fig. 6.

We note, however, that the cases of nonmonotonic profiles have now received only our moderate attention as yet. They call for further investigation.

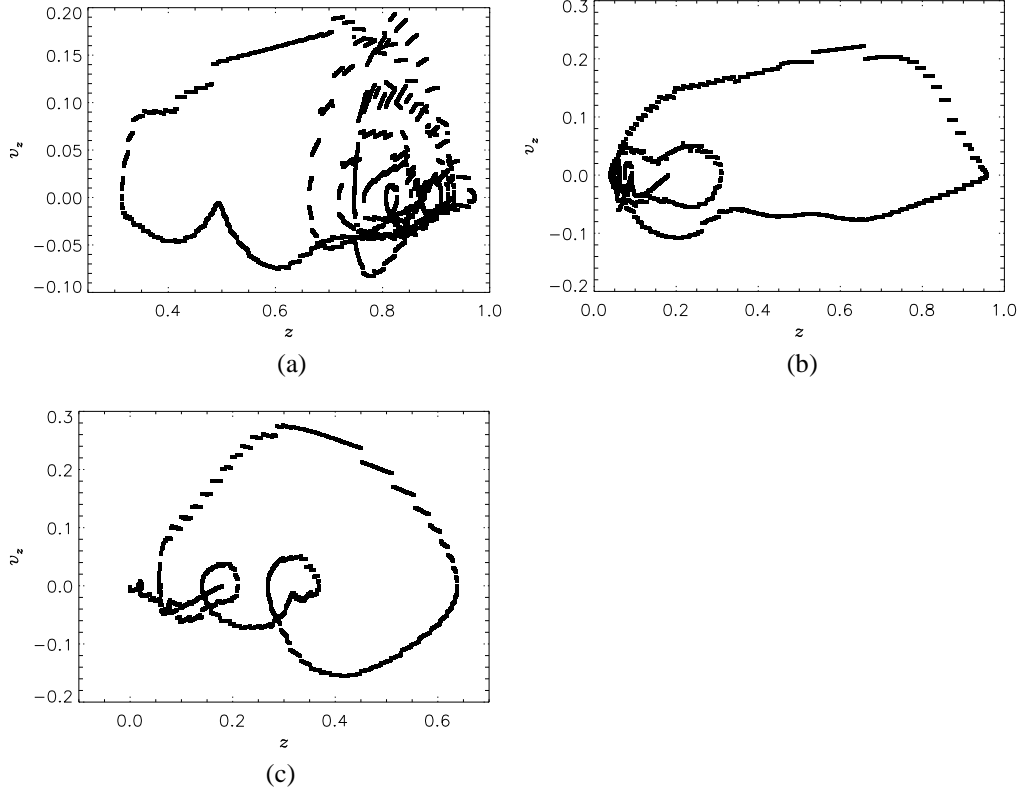


Figure 6: Phase trajectories of different fluid particles in the problem with a nonmonotonic static temperature profile.

4. Conclusion

We see that the stratification due to the variable thermal diffusivity, with a sharp kink in the static temperature profile, can give rise to the development of small-scale flows superposed onto larger-scale flows, i.e., on the whole, to the splitting of convection scales. In the case of two rigid boundaries, small-scale cells are localised in both the upper and bottom boundary sublayers. However, small-scale cells are observed only near the upper boundary, if it is free. In this case, harmonics with different wavenumbers dominate at different heights, and a type of intermittency takes place: the enhancement of the small-scale component is frequently accompanied by the weakening of the large-scale component and vice versa, so that the flow pattern is on the whole far from stationary. In both cases, the thickness of the localisation zones of small-scale cells exceeds the thickness of the sublayer with a sharp temperature change, Δh . Small cells are carried by large-scale flows; if the upper boundary is free, this process appears as the sinking of small cells. Moreover, the appearance of phase trajectories in the case of a nonmonotonic profile can also be interpreted as a manifestation of the transfer of small-scale structures by the large-scale flow. It is worth noting in this context that, as some observational data suggest, granules are carried by larger-scale flows in the solar convection zone. Analyses of correlations between the brightness variations at two points located not far from each other suggest that granules may

even repeatedly emerge on the solar surface, playing a relatively passive role in the convection dynamics (Getling, 2006).

Clearly, the simplified models considered here cannot offer a realistic description of solar convection, the structure of which depends on a multitude of factors, such as the density difference across the convection zone, the complex thermal stratification, the complex equation of state of the matter (related to the variable ionization degree), radiative heat exchange, etc. Nevertheless, such models are instructive in terms of evaluating the possible role of various factors in the formation of the real pattern.

Acknowledgement

This work was supported by the Russian Foundation for Basic Research, project 12-02-00792-a.

References

- Arakawa, A., Computational design for long-term numerical integration of the equations of fluid motion: Two-dimensional incompressible flow. Part I, *J. Comput. Phys.*, 1966, 1, 119-143; reprinted: 1997, 135, 103-114 (CP975697).
- Blahut, R. E., *Fast Algorithms for Signal Processing*, Addison-Wesley, Boston, 1985.
- Getling, A. V., Convective motion concentration at the boundaries of a horizontal fluid layer with inhomogeneous unstable temperature gradient along the height, *Fluid Dyn.* 1976, 10, 745-750.
- Getling, A. V., Scales of convective flows in a horizontal layer with radiative transfer, *Izv., Atmosph. Oceanic Phys.*, 1980, 16, 363-365.
- Getling A. V., *Rayleigh-Bénard Convection: Structures and Dynamics*, World Scientific, Singapore, 1998; URSS, Moscow, 1999.
- Getling, A. V., Do quasi-regular structures really exist in the solar photosphere? I. Observational evidence, *Solar Phys.*, 2006, 239, 93-111.
- Getling, A. V., & Tikhomolov, E. M., Scale splitting in solar convection, *Trudy XI Pulkovskoi mezhdunarodnoi konferentsii po fizike Solntsa* (Proc. 11th Pulkovo Int. Conf. on Solar Physics), Pulkovo, 2007, pp. 109-112.
- Kovenya, V. M., & Yanenko, N. N., *The Splitting Method in Problems of Gas Dynamics*, Novosibirsk, Nauka, 1981.
- Krishan, K., Kurtuldu, H., Schatz, M. F., Madruga, S., Gameiro, M., & Mischaikow, K., Homology and symmetry breaking in Rayleigh-Bénard convection: Experiments and simulations, *Phys. Fluids*, 2007, 19, 17105.
- Mazhorova, O. S., & Popov, Yu. P., Methods for the numerical solution of the Navier-Stokes equations, *USSR Comput. Math. Math. Phys.*, 1980, 20, 202-217.
- Mazhorova, O. S., & Popov, Yu. P., Matrix iteration method of numerical solution of Navier-Stokes two-dimensional equations, *Doklady Akademii nauk SSSR*, 1981, 259, 535-540.